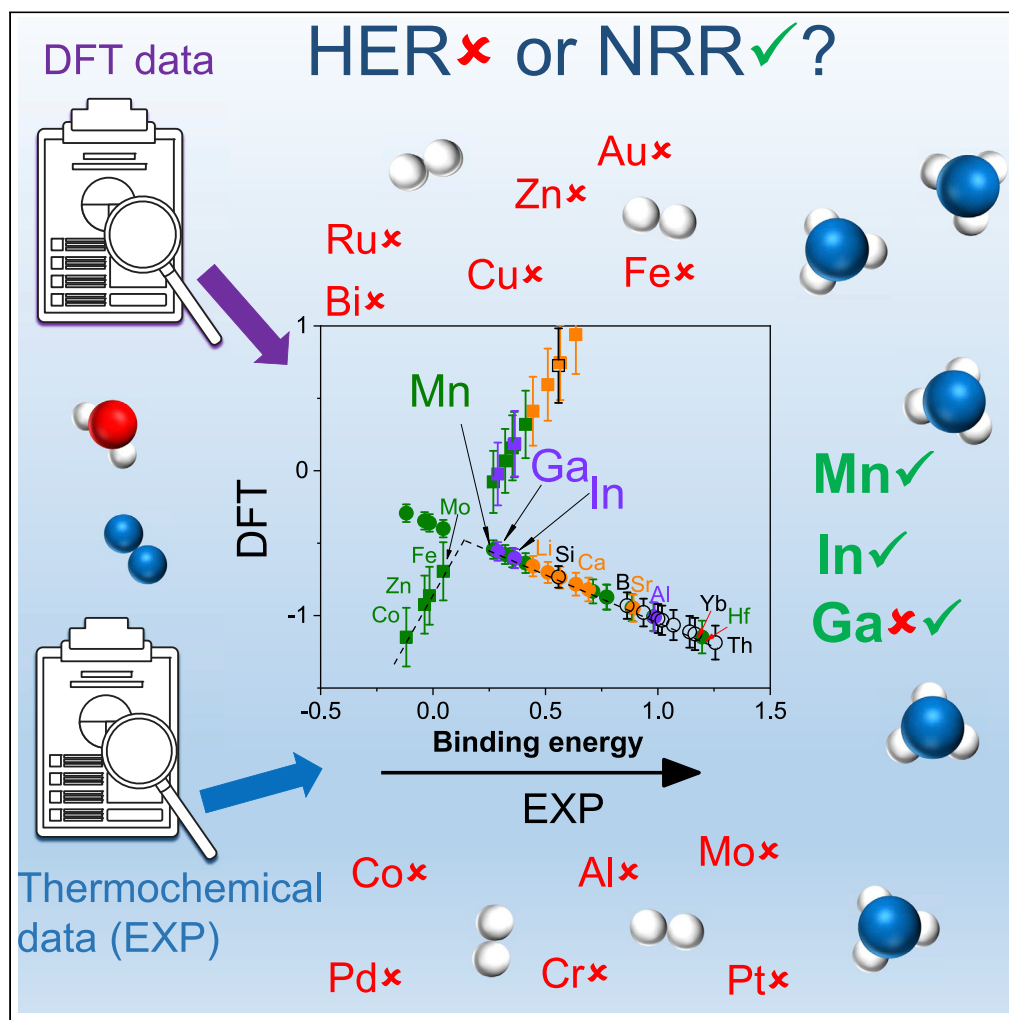


Article

Are There Any Overlooked Catalysts for Electrochemical NH_3 Synthesis—New Insights from Analysis of Thermochemical Data

Emil Dražević,
Egill Skúlason

edrazevic@eng.au.dk

HIGHLIGHTS

New descriptors for NRR from experimental thermochemical data established

Largest NRR volcano plot to date with a gap of unidentified materials at the top

Mn, Ga, and In are overlooked catalysts that can selectively catalyze NRR

Our results can be used to identify false-positives in the literature

Dražević & Skúlason, iScience
23, 101803
December 18, 2020 © 2020
The Author(s).
<https://doi.org/10.1016/j.isci.2020.101803>

Article

Are There Any Overlooked Catalysts for Electrochemical NH₃ Synthesis—New Insights from Analysis of Thermochemical DataEmil Dražević^{1,3,*} and Egill Skúlason²

SUMMARY

We report relations between nitrogen-binding-energy descriptors obtained from experimental thermochemical data and limiting potentials from density functional theory data. We use the relations to build the largest volcano plot for nitrogen reduction reaction (NRR). We found that (1) Mn, Ga, and In are overlooked catalysts and (2) there are unidentified materials on the top of the volcano. Using experimental exchange current densities of hydrogen evolution reaction (HER) and Pourbaix diagrams we have identified conditions at which Mn, Ga, and In remain stable in water and selectively catalyze NRR over HER. We found that Fe, Au, Cu, Bi, and Pd, on contrary to what was reported earlier, need smaller applied potentials to start the onset of HER than NRR in water. We make a critical discussion about them and other candidates and we believe our results can be used to identify false positive measurements in the research field.

INTRODUCTION

Ammonia (NH₃) can be synthesized using renewable energy and the abundant resources of water and nitrogen, with no need for co-location, unlike carbon-based fuels originating, e.g., from CO₂ reduction, which need to be collocated with CO₂ sources. Ammonia's main uses are in agriculture and the refrigeration industry (Appl, 2011), but there is a growing interest to use it as a fuel. NH₃ can be produced in a sustainable manner with no CO₂ emissions by combining a renewable-energy-powered electrolyzer and a Haber-Bosch reactor. Such "green" process would enable the agricultural industry to base its growth on CO₂-neutral fertilizers. Due to large heat losses at small scales, Haber-Bosch is more suitable for larger scales >100 kg h⁻¹ (Rouwenhorst et al., 2019).

Alternatively, NH₃ can be synthesized in an electrochemical reactor, a process most likely highly suitable for smaller scales (Deng et al., 2018; Macfarlane et al., 2020; Comer et al., 2019). Here on the cathode, hydrogen in the form of H⁺ and e⁻ reduces N₂ stepwise to NH₃ (Skúlason et al., 2012). The research field is plagued with a number of false-positive measurements, which is the reason why rigorous experimental protocols have been published recently (Andersen et al., 2019; Greenlee et al., 2018; Hanifpour et al., 2020; Tang and Qiao, 2019; Suryanto et al., 2019). Earlier works or reports that do not follow the protocols and produce large amounts of NH₃, and yet claim high efficiencies, should be taken with a great level of a precaution.

The electrochemical synthesis is hampered by the lack of a suitable cathode material that can selectively catalyze N₂ to NH₃ at practically usable production rates (Chen et al., 2017; Guo et al., 2018a; Giddey et al., 2013; Foster et al., 2018). The electrocatalyst's reaction selectivity is governed by the competition between the adsorption of nitrogen and protons. Theoretically, the best catalysts are transition metals, and among them the most reactive are Mo, Fe, and Ru (Skúlason et al., 2012; Montoya et al., 2015). The electrocatalyst's reaction selectivity is governed by the competition between the adsorption of nitrogen and protons. However, the d-orbital electrons make most of the transition metals better binders of protons than nitrogen at reducing conditions. The potentials needed to start the onset of the NRR are also more negative than for the hydrogen evolution reaction (HER). (Chen et al., 2017; Guo et al., 2018a; Giddey et al., 2013; Foster et al., 2018). This all together results in a Faradaic efficiency (FE) often below 1% for nitrogen reduction reaction (NRR) on Ru, Fe, and Mo in aqueous media (Foster et al., 2018; Kyriakou et al., 2017). A slightly higher FE was reported using other d-metals such as V (Kyriakou et al., 2020), Co (Guo et al., 2018b), Au (Hao et al., 2019), and Cu (Lin

¹Aarhus University, Department of Biological and Chemical Engineering, Aabogade 40, 8200 Aarhus N, Denmark

²Egill Skúlason, University of Iceland, Science Institute and Faculty of Industrial Engineering, Mechanical Engineering and Computer Science, Hjarðarhagi 2, VR-III, 107 Reykjavík, Iceland

³Lead Contact

*Correspondence: edrazevic@eng.au.dk
<https://doi.org/10.1016/j.isci.2020.101803>



et al., 2019). Beside transition metals, some s-block elements were exploited as catalysts in NH_3 synthesis, either using thermal and electrothermal cycling strategies or in electrochemical synthesis (classical heterogeneous electrocatalysis) (Appl, 2011; Singh et al., 2017; Mccanney et al., 2017; Schwalbe et al., 2020; Akira et al., 1993). Cycling strategy should not be confused with heterogeneous electrocatalysis as it does not involve proton-coupled electron transfers (PCET) and adsorbed intermediates but rather electron and proton transfers occurring separately in two different steps. Thermal cycling process was one of the first industrial process for ammonia synthesis, the Frank-Caro process (Appl, 2011). It used CaC_2 to fix N_2 as Ca-cyanamide (electron transfer). Ca-cyanamide was subsequently hydrogenated with water (proton transfer) to form NH_3 and CaCO_3 . CaCO_3 could be recycled afterward to CaC_2 by reducing it at high temperatures with carbon (electron transfer). Li electro-thermal cycling has recently been introduced as a strategy for producing NH_3 reporting FE of 89% (Mccanney et al., 2017), where proton and electron transfer occur in separate steps. Li was also exploited as a catalyst in the electrochemical synthesis of NH_3 in non-aqueous media with limited concentration of protons where it is hypothesized that heterogeneous catalysis is occurring, i.e., NRR involves PCETs (Singh et al., 2017, 2019; Akira et al., 1993; Schwalbe et al., 2020). In that case the FE is 10% and much lower than in Li-cyclic process. The largest drawbacks of Li-electrocatalysis in non-aqueous solvents are low FE and cell potentials of around 4 V, which make energy consumption roughly around 10 times higher than that of conventional Haber-Bosch (Andersen et al., 2019; Akira et al., 1993; Schwalbe et al., 2020). It would be therefore beneficial to identify catalysts beyond Li in non-aqueous media where NRR could occur at lower overpotentials and higher FE. With respect to other catalysts, a post-transition metal, Bi, was claimed recently to selectively catalyze NRR (65% FE) at very high production rates in potassium-based aqueous electrolytes (Hao et al., 2019). The result is likely a false-positive and might be attributed to NO_x reduction and not N_2 reduction (Choi et al., 2020).

Most of the studies performed to date in the field of electrochemical synthesis (heterogeneous catalysis) of NH_3 used similar catalysts (a few different transition metals and Li) in aqueous, non-aqueous, and molten-salt electrolytes with limited or no success (Andersen et al., 2019). New theoretical works deem non-aqueous electrolytes as a pathway to higher selectivity; however, this is yet to be experimentally confirmed (Singh et al., 2019; Schwalbe et al., 2020; Zhou et al., 2017). Notwithstanding electrochemical synthesis of NH_3 is performed in aqueous or non-aqueous media, the field lacks new catalysts, beyond Fe and Li, which can properly address the selectivity challenge. Our contribution to the field is in answering the following important research question: Are there any overlooked catalysts that help the field move forward? To answer the question above, we perform here perhaps one of the most extensive screening study, which includes metals originating from s-, d-, p-, lanthanides, and actinides blocks of periodic system of elements of possible catalysts for NRR. We use a genuine approach where we relate experimental thermochemical data of nitride formation to limiting potentials from earlier density functional theory (DFT) studies and use the new relations to identify new catalysts. We use standard enthalpies and entropies of nitride formations to calculate the new descriptors - Gibbs free energies of pure metal nitridation. These were experimentally measured in the last century for many elements. The reaction pathways for NRR and limiting potentials were computed earlier for a range of transition metals using DFT calculations (Skúlason et al., 2012). The potential determining step (PDS) and the potential needed to have all the reactions steps downhill can be deduced from such calculations. This simple implicit electrochemical model, incorporated with scaling relations of adsorbed intermediates and adsorption energy descriptors (Abild-Pedersen et al., 2007), has been shown to agree with experimentally measured potentials to start the onset for several electrocatalytic reactions, including hydrogen evolution reaction (HER) (Nørskov et al., 2005; Greeley et al., 2006; Skúlason et al., 2010), oxygen reduction reaction (ORR) (Nørskov et al., 2004; Greeley et al., 2009; Gislason and Skúlason, 2019), NRR (Skúlason et al., 2012; Montoya et al., 2015), and CO_2 reduction reaction (CO_2RR) (Kuhl et al., 2014; Peterson et al., 2010; Peterson and Nørskov, 2012; Hussain et al., 2018). Furthermore, more advanced modeling of the kinetics involved in NRR on Ru has shown that the thermochemical barriers are sufficient to capture the limiting potentials as additional barriers are low (Tayyebi et al., 2019).

At the end we compared the potentials needed to start the onset of HER and NRR at different pH and on different pure metal catalysts. We critically discuss our data in comparison with some earlier reported experimental works.

RESULTS AND DISCUSSION

Potential Determining Steps and Limiting Potentials for NRR

Electrochemical NRR, which is of interest here, can follow two different reaction pathways, associative and dissociative Heyrovsky pathways, as depicted in Figure 1 (Skúlason et al., 2012). The pathways include initial

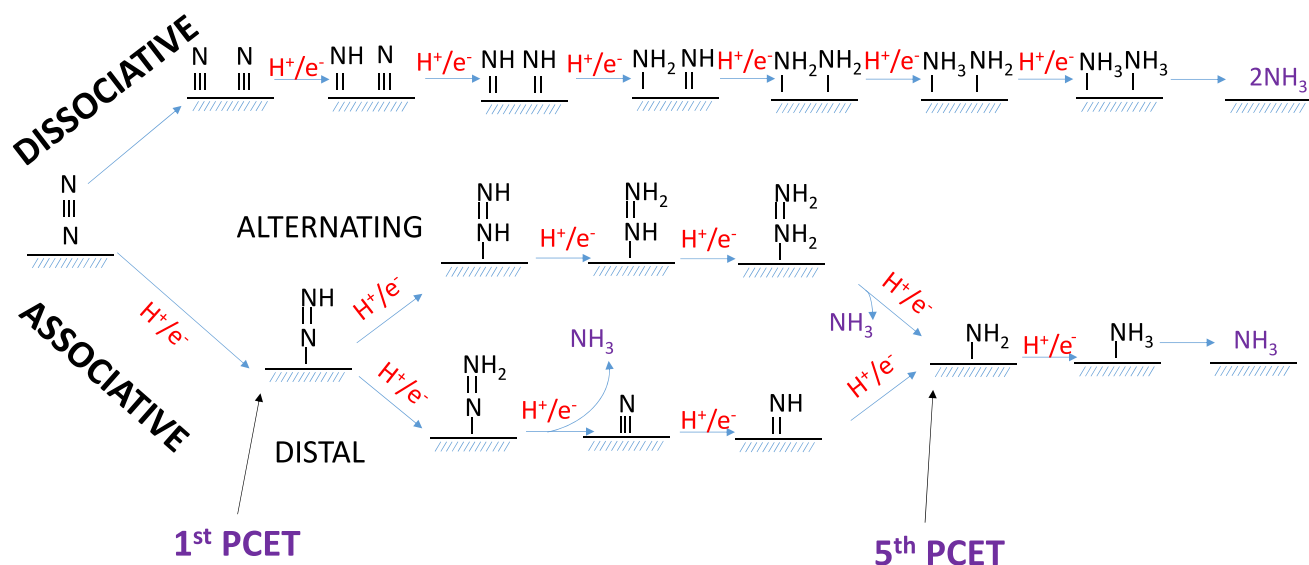


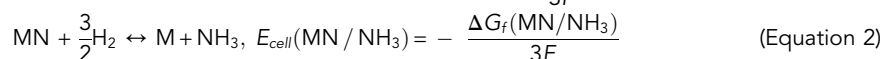
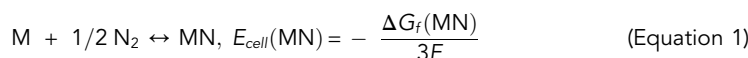
Figure 1. Reaction Pathways of NRR

Two mechanisms are possible: a dissociative mechanism where N_2 is first dissociated on the surface before the atomic N is reduced further to NH_3 and an associative mechanism where adsorbed N_2 is directly protonated to two NH_3 molecules. Two possible reaction pathways are possible via the associative mechanism: an alternating pathway and a distal pathway, depending on which N atom of the N_2 molecule is protonated. Two key reaction steps are indicated for the proposed mechanism at ambient conditions of the distal associative mechanism, the first proton-coupled electron transfer (PCET) step and the fifth PCET step, which have been predicted to be the PDS on transition metal surfaces (Skúlason et al., 2012).

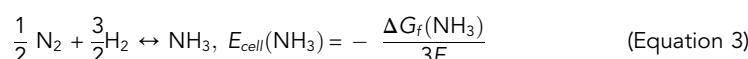
adsorption of N_2 , six PCET steps, and desorption of two NH_3 molecules after which the metal surface is clean and the catalytic cycle is completed. At room temperatures, which is the case for the electrochemical processes investigated here, the rate at which dissociative pathway occurs is very low. NRR at low temperatures and the weak N-binding metals predominantly follow the Heyrovsky associative pathway (Skúlason et al., 2012). For the strong N-binding metals the Heyrovsky dissociative pathway may also be favored. In case of weak N-binding transition metals NRR follows either the distal or alternating associative pathway. The PDS are either the first or fifth PCET (marked in Figure 1), depending on the physicochemical nature of the catalyst (Skúlason et al., 2012). The predicted limiting potentials for NRR are available for a range of transition metals, and they scale linearly with N-binding energy ($\Delta E(N)$) of a certain catalyst (Skúlason et al., 2012). In this study we do not perform any new DFT calculations but use the data (limiting potentials and N-binding energies) from a previously published study (Skúlason et al., 2012). In the Supplemental Information we define our notations of key terms used in this work such as limiting potentials, overpotentials, onset potentials, E_{cell} , and PDS, which may vary between different research fields, but we have used the same notations of the electrical potential terms as in the work of Peterson and Nørskov (2012).

$E_{cell}(MN)$ and $E_{cell}(MN/NH_3)$ as Experimental Descriptors of N-Binding Energy

In the Transparent Methods section, how new N-binding energy descriptors, $E_{cell}(MN)$ and $E_{cell}(MN/NH_3)$, are calculated has been described. Briefly, we use two reaction steps below to explain the new descriptors:



Equation 1 is the standard MN formation from N_2 and M, where standard Gibbs free energy of formation ($\Delta G_f(MN)$) is referenced to N_2 . Equation 2 corresponds to the reverse reaction, where MN is hydrogenated to form M and NH_3 and corresponding $\Delta G_f(MN/NH_3)$ is referenced to NH_3 . Equations 1 and 2 summed up together give the standard Gibbs free energy of formation of ammonia:



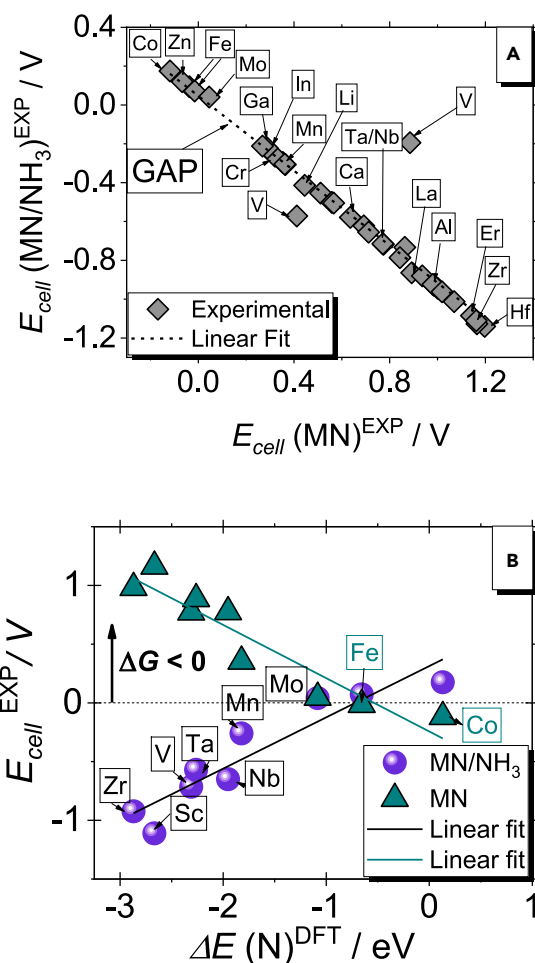


Figure 2. The New Experimental Descriptors of NRR

(A) $E_{cell}(MN)$ and $E_{cell}(MN/NH_3)$ plotted against each other. Dashed line is the linear fit, which includes all data points with the following equation: $E_{cell}(MN/NH_3) = -0.96 E_{cell}(MN) + 0.04$, $R^2 = 0.91$.

(B) $E_{cell}(MN)$ and $E_{cell}(MN/NH_3)$ data calculated as described in the [Transparent Methods](#) section (The cell potential of M to MN reaction and The cell potential of MN reaction with H_2 to form NH_3 and metal), plotted against $\Delta E(N)$ calculated in reference ([Skúlason et al., 2012](#)) for flat metal surfaces. The linear equations above are as follows: $E_{cell}(MN) = (-0.45 \pm 0.06) \Delta E(N) - (0.24 \pm 0.12)$, $R^2 = 0.87$ and $E_{cell}(MN/NH_3) = (0.43 \pm 0.06) \Delta E(N) - (0.31 \pm 0.12)$, $R^2 = 0.85$. Superscripts EXP and DFT mark experimentally obtained thermochemical data and theoretical DFT data, respectively. The arrow above the dashed line indicates an area where $\Delta G < 0$.

We choose to express $\Delta G_f(kJ mol^{-1} NH_3)$ as E_{cell}/V , where 3 is the number of electrons involved and F is the Faraday's constant. Half-cell reactions of [Equations 1](#) and [2](#) are found in the [Transparent Methods](#) section. Now, from [Equations 1](#), [2](#), and [3](#), $E_{cell}(NH_3) = E_{cell}(MN) + E_{cell}(MN/NH_3) = 0.0566 V$, a relation valid for all elements in the periodic system of elements that form nitrides. If $E_{cell}(MN)$ is very positive, M is a very strong N binder, and $E_{cell}(MN/NH_3)$ will be $0.0566 V - E_{cell}(MN)$, i.e., very negative.

[Figure 2A](#) plots $E_{cell}(MN/NH_3)$ against $E_{cell}(MN)$ for all 31 elements analyzed in this study. We observe a highly linear correlation, which has a slope of -0.96 and an intercept of $0.04 V$. Vanadium points clearly stick out as outliers. Two V points are found in the plot because we analyzed two types of vanadium nitrides, V_2N and VN . This was also the case with some other metals, e.g., Fe, Mn, Ta, and Nb, which also form several types of nitrides (36 nitrides, 31 elements, see [Supplemental Information Table S1](#)). The reason for V being an outlier could be very imprecise measurements of standard enthalpies and entropies of formation of vanadium nitrides. If V would be taken out from [Figure 2A](#), the square of correlation coefficient R^2 would increase from 0.91 to 1.00, the slope then becomes -1.00 and the intercept $0.06 V \approx 0.0566 V = E_{cell}(NH_3)$. According to Sabatier principle, an ideal catalyst will bind the key reaction intermediate with just the

perfect strength. The relation in Figure 2A can be used to give a rough idea on good catalysts, as good catalysts preferably will have slightly positive $E_{\text{cell}}(\text{MN})$, as it is preferable that they bind N well, but not too well, as we want to invest minimum work uphill $E_{\text{cell}}(\text{MN}/\text{NH}_3) = 0.0566 \text{ V} - E_{\text{cell}}(\text{MN})$ to desorb N in the form of ammonia leaving a clean M surface ready for a new catalytic cycle. As an upper limit, values of $E_{\text{cell}}(\text{MN}) < 0.4 \text{ V}$ might also appear interesting. The catalysts that are in this range are Mo, Mn, Ga, In, Cr, and Li, where Ga, Mn, and In appear as new candidates.

What is quite important to note here is that we detect a large gap of elements in the range of $0.05 \text{ V} < E_{\text{cell}}(\text{MN}) < 0.29 \text{ V}$, and here lie potentially most promising unidentified catalysts. It is highly likely that elements in the gap exist in the periodic system of elements, but for some reason the thermochemical data for their nitride formation has not been measured yet.

The calculated limiting potentials in NRR scale linearly with nitrogen binding energy $\Delta E(\text{N})$. If $E_{\text{cell}}(\text{MN})$ and $E_{\text{cell}}(\text{MN}/\text{NH}_3)$ scale linearly with DFT-calculated $\Delta E(\text{N})$, it would mean that the limiting potentials must also scale linearly with $E_{\text{cell}}(\text{MN})$ and $E_{\text{cell}}(\text{MN}/\text{NH}_3)$. Figure 2B compares $E_{\text{cell}}(\text{MN})$ and $E_{\text{cell}}(\text{MN}/\text{NH}_3)$ with $\Delta E(\text{N})$ for transition metals (Skúlason et al., 2012). Although the data show a certain degree of scattering, both cell potentials correlate linearly with theoretically calculated N-binding energies. Figure 2B is in fact a volcano plot, built using our new descriptors and DFT-calculated N-binding energy on transition metals. In Figure 2B, for each $\Delta E(\text{N})$ we have $E_{\text{cell}}(\text{MN}) + E_{\text{cell}}(\text{MN}/\text{NH}_3) = 0.0566 \text{ V}$. The intersect and area around it is where both E_{cell} are minimal, and here potentially most promising candidates lie. The intercept of the two mirror-image-like linear fits is the top of the volcano, here the Fe catalyst. However, given the scattering, the top of the volcano could be anywhere in the Fe-Mo area. We note that no limiting potentials from DFT are taken into account in Figure 2B, and as such it gives only an idea where good catalysts would appear.

Figure 3 plots the limiting potentials (U_L) calculated earlier on transition metal surfaces against their $E_{\text{cell}}(\text{MN})$ and $E_{\text{cell}}(\text{MN}/\text{NH}_3)$. We observe linear correlations, against both new N-binding energy descriptors. The data are scattered, but the squared correlation coefficients R^2 are relatively high and ranging from 0.85–0.87 to 0.91–0.92, for the fifth and first PCET, respectively. Scattering can be attributed to the imprecision of DFT in determining the limiting potentials (Kepp, 2018) and any experimental uncertainties related to thermochemical data of formation of different metal nitrides. This is the first time such DFT-EXP relations are reported for a range of elements. These relations confirm the DFT-obtained N-binding energies for a range of metals correlate very well with experimental ΔG_f obtained from in Equations 1 and 2. It is highly likely that similar DFT-EXP relations will also be established for, e.g., H-binding, O-binding, and C-binding elements.

Figures 3A and 3B are mirror images, have a shape of a typical volcano plot, and show the same trends. The reason for the figures being mirror-like is in the relation $E_{\text{cell}}(\text{MN}) + E_{\text{cell}}(\text{MN}/\text{NH}_3) = 0.0566 \text{ V}$. $E_{\text{cell}}(\text{MN})$ is proportional to the increase in the N-binding energy, whereas $E_{\text{cell}}(\text{MN}/\text{NH}_3)$ is inversely proportional to the increase in N-binding energy as shown in Figure 2B. It should be noted that even though the two descriptors involve nitride formation followed by reduction and hydrogenation of the nitride to ammonia and M, it does not mean this is the overall mechanism we propose here. The mechanism is given by a classical heterogeneous PCET process on metal catalysts as shown in Figure 1, and this is also why we searched for the relations between the limiting potentials and the new descriptors in Figure 3. The present study should not be confused with earlier study where transition metal nitrides were computationally screened for NRR using a Mars-van Krevelen mechanism (Abghoui et al., 2015). In the next section, we use the linear relations obtained in Figure 3A as “calibration curves” and estimate the unknown limiting potentials for all other elements from their known $E_{\text{cell}}(\text{MN})$, values that are found in Supplemental Information and Table S2.

A Volcano Plot Built from Estimated NRR Limiting Potentials versus Experimental $E_{\text{cell}}(\text{MN})$

In this section we present, to our knowledge, the largest volcano plot for NRR, which includes s-metals, transition metals, post-transition metals, and elements from p-block, lanthanides, and actinides, shown in Figure 4. More detailed insight into specific elements and the data presented in Figures 3 and 4 can be found in Supplemental Information and Table S2.

Lanthanides and actinides are among the strongest binders of nitrogen and are placed on the right side of the volcano plot, where the PDS is the fifth PCET. Their NRR limiting potential decreases with the increase in atomic weight (it is more negative). The actinide metal Th is the strongest N binder of all elements

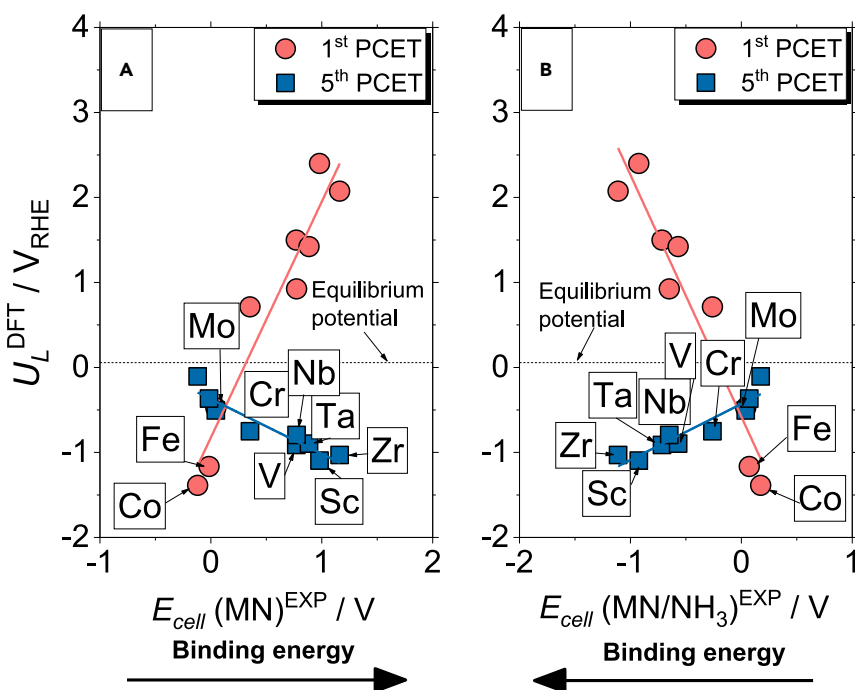


Figure 3. NRR Limiting Potentials versus the New Experimental Descriptors

U_L were calculated using N-binding energies (Skúlason et al., 2012) and substituting them in equations: (1) first PCET, $U_{L,1}$ (Y-Fe) = $1.61 \cdot \Delta E(N) + 2.22$, and $U_{L,1}$ (Fe-Ag) = $0.59 \cdot \Delta E(N) + 1.31$, and (2) fifth PCET $U_{L,5} = -0.33 \cdot \Delta E(N) + 0.15$ (Skúlason et al., 2012). Superscripts EXP and DFT mark experimentally obtained thermochemical data and theoretical DFT data, respectively. Dashed line is the equilibrium potential.

(A) U_L versus E_{cell} (MN). The colored solid lines are the corresponding linear fits that have the following equations: first PCET $U_L = (2.77 \pm 0.29) E_{cell} (MN) - (0.82 \pm 0.20)$, $R^2 = 0.92$ and fifth PCET $U_L = (-0.65 \pm 0.08) E_{cell} (MN) - (0.37 \pm 0.06)$, $R^2 = 0.87$.

(B) U_L versus E_{cell} (MN/NH₃). The colored solid lines are the corresponding linear fits that have the following equations: first PCET $U_L = (-2.84 \pm 0.33) E_{cell} (MN/NH_3) - (0.58 \pm 0.19)$, $R^2 = 0.91$ and fifth PCET $U_L = (0.66 \pm 0.09) E_{cell} (MN/NH_3) - (0.42 \pm 0.06)$, $R^2 = 0.85$. The arrows indicate a direction where N-binding energy is increasing.

analyzed in this study. In general, elements from these groups do not appear interesting for NRR in water, because of their limited abundance, radioactivity, and often instability in water media (Greenwood and Earnshaw, 1997).

s-block elements are also placed on the right leg. We observe a very clear and a regular trend of increase in NRR reactivity as follows: Be-Mg-Ca-Sr-Ba-Li, with lithium being the most reactive catalyst. Li is also the weakest N binder among s-metals, very electropositive element, and Li-N bonds in Li₃N have a strong ionic character (Greenwood and Earnshaw, 1997). Li therefore releases N much easier than other s-metals. The bonds of other s-metals have a more covalent character, although they are all considered “salt-like” nitrides. For example, earth-alkali elements tend to form MN bonds with a less “salt-like” character where Be₃N₂ has the least “salt-like” character and is most stable (Greenwood and Earnshaw, 1997). This is best seen by comparing the thermal stability where, e.g., Be₃N₂ melts at 2,200°C, whereas Mg₃N₂ decomposes above 271°C. Evidences of existence of sodium nitride and some other alkali metal nitrides are not available (Greenwood and Earnshaw, 1997). In fact, it is not verified that Na and K form nitrides but rather azides, NaN₃ or KN₃ (Greenwood and Earnshaw, 1997). Interestingly, CaC₂ and Li were exploited as catalysts in NH₃ synthesis using cycling strategies, e.g., CaC₂ in Frank-Caro process or Li-cycling strategy, where electron and proton transfers occur in two separate steps (Appl, 2011, Mccanney et al., 2017).

Furthermore, Li has been used as catalyst in continuous electrochemical synthesis of NH₃ in non-aqueous media with ethanol as a proton source. However, at this point it is not clear if this process involves any heterogeneous electrocatalysis mechanism depicted in Figure 1 or if it occurs in separate Li nitridation (electron transfer) and then Li nitride hydrogenation (proton transfer) steps without involving any adsorbed N_xH_y

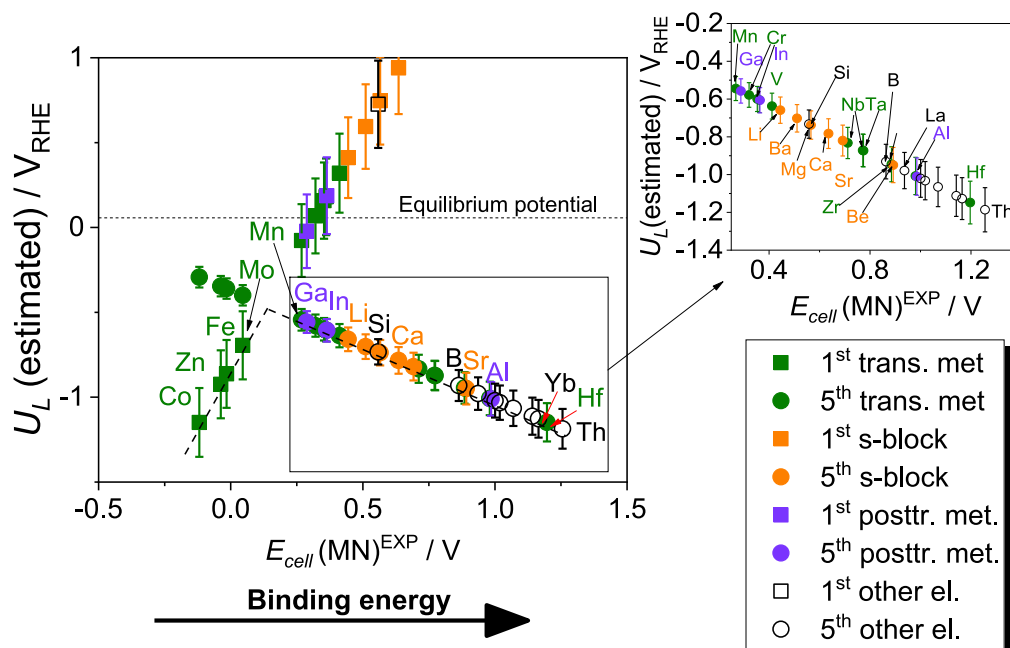


Figure 4. Volcano Plot for 31 Different Elements

Estimated limiting potentials U_L values for first and fifth PCET were calculated using the linear relations obtained in Figure 3A and E_{cell} (MN) values. The propagation errors were calculated from the corresponding errors associated with the slopes and intercepts from Figure 3A: $err(U_L(1^{st})) = \sqrt{(E_{cell}(MN) * 0.29)^2 + 0.2^2}$ and $err(U_L(5^{th})) =$

$\sqrt{(E_{cell}(MN) * 0.08)^2 + 0.06^2}$. All related data are found in Supplemental Information and Table S2. Dashed lines are added to guide the eye. Symbol color and font color match the catalyst coming from a certain group, e.g., green font and symbols are for transition metals. Squares are first PCET, and circles, fifth PCET. "Others" in the plot are non-metals B and Si from the p-block and some metals from lanthanides and actinides blocks. The black arrow shows in which direction N-binding energy increases. Dashed-dotted horizontal line is the equilibrium potential of ammonia formation.

species and PCETs (Schwalbe et al., 2020). The potential of $-3.8 V_{RHE, pH 0}$ was applied, which is much more negative than what we predict in Figure 4. It is hypothesized here that due to the lack of protons (ethanol as the proton source, $pK_a = 16$, proton concentration $\approx 10^{-16}$ mol/L) the mechanism is rather Li cycling than heterogeneous catalysis involving PCET as shown in Figure 1. This would explain the need for applied potentials being more negative than Li^+/Li standard reduction potential ($-3.04 V_{RHE, pH 0}$).

Transition metals span over the whole volcano plot. Most transition metals studied here are found on the right leg of the volcano plot. Only Zn, Co, Fe, and Mo are present on the left leg and are limited by the first PCET because they weakly bind nitrogen. Hf and Zr are placed far out on the right leg as the strongest N binders. Other transition metals, which are known to be on the left leg (weak N binders), and whose experimental thermochemical data on nitride formation are not available, are Ru, Rh, Pt, Pd, Cu, Ag, and Au (Skúlason et al., 2012; Guo et al., 2018a; Montoya et al., 2015). We find Mn the most reactive transition metal catalyst for NRR, followed by Mo, Fe, and Cr. Interestingly, Mn can promote NRR better than Mo, Fe, and Ru. Overall it is the most reactive catalyst and appears overlooked as a catalyst for NRR. We note here that there is a gap of materials at the top, and that an unidentified material at the top, if exists, can outperform Mn. We also note that the best performing materials should bind N more strongly than Fe or Mo, and here we identify that the best performing materials will have E_{cell} (MN) = 0.12 V and corresponding limiting potential will be a bit above $-0.5 V_{RHE}$ (work needed is around 140 kJ/mol NH_3). We predict here that elements on the top of the volcano will never have overpotential lower than around 0.60 V. However, it should be noted here that we use limiting potentials from pure metals as "calibration curves" (Skúlason et al., 2012). Therefore, our predictions are limited by the scaling relations for pure metals. It is, however, possible to break these scaling relations with other types of materials, such as ceramics of, e.g., metal sulfides (Abghoui et al., 2019). Here RuS_2 was predicted to be at the top of the volcano with around 0.35 V in overpotential. However, it binds protons stronger than nitrogen, and thus HER will prevail.

Post-transition metals are poor catalysts for HER, which could be beneficial for selectivity of NRR over HER (Han et al., 2020). A post-transition metal, Bi, was recently reported to catalyze NRR very selectively (65%) at only $-0.7 V_{\text{RHE}}$ in potassium-ion-based aqueous electrolytes (Hao et al., 2019). Unfortunately, we could not find any thermochemical data on bismuth nitride formation to be able to plot it on Figure 4. However, the limiting potential found using DFT in the same study was as low as $-2.63 V_{\text{RHE}}$ (Hao et al., 2019). It does not appear possible to produce NH_3 from N_2 at $-0.7 V_{\text{RHE}}$ using Bi as electrocatalyst in aqueous media. It is likely that the work on Bi is a false-positive and the authors have been reducing NO_x impurities in N_2 gas and not N_2 itself on Bi catalyst (Choi et al., 2020). We find here that In and Ga, are quite close to the top of the volcano plot, and to our knowledge they have not been tested yet as electrocatalysts for NRR. They are very interesting candidates for NRR as they are strong binders of N and poor catalysts for HER. Galinstan, an alloy of Ga, In, and Sn, was reported to effectively catalyze the reduction of nitrophenols ($-\text{NO}_2$) to aminophenols ($-\text{NH}_2$) with NaBH_4 in water, which is a 6 PCET electrochemical reaction step (Hoshyargar et al., 2015). However, the reduction of nitro groups does not include breakage of the triple bond. Yet, positive values of $E_{\text{cell}}(\text{MN})$ for Ga and In indicate that they bind nitrogen stronger than Fe or Mo, which makes them highly promising for NRR. Aluminum is the strongest binder of nitrogen of post-transition metals analyzed here. Aluminum nitride is a known by-product in aluminum production, which can be found in the waste product called “salt-cake” (Bruckard and Woodcock, 2007). The presence of AlN in the “salt-cake” is hazardous as it reacts with moisture in the air to form NH_3 and aluminum oxide (Bruckard and Woodcock, 2007). Siemens has recently filed a patent proposing Al catalyst in electrochemical synthesis of NH_3 (Reller et al., 2018). However, it is unclear if the process involves any classical heterogeneous catalysis mechanism (Reller et al., 2018). Nevertheless, Al does appear as an interesting candidate for heterogeneous catalysis in electrochemical synthesis of NH_3 as Al is a known poor HER promoter (Trasatti, 1972). In the next section we further analyze NRR over HER selectivity in water for the most promising catalysts from Figure 4, i.e., Mo, Mn, Ga, In, Cr, and Al, and some other metals that were reported to successfully promote NRR in water.

Potentials Needed to Start the Onset of NRR and HER in Aqueous Media at Different pH

The rate of HER and the potential at which HER occurs depend on the H-binding energy (Skúlason et al., 2010; Nørskov et al., 2005; Trasatti, 1972) of the catalyst and the pH. Figure 5A is a volcano plot for HER reproduced from an earlier experimental work, which plots the exchange current of HER versus the H-binding energy of the metal (MH), i.e., heat of adsorption of H_2 gas on these metals (Trasatti, 1972). Naturally, catalysts that bind H poorly would appear as a good choice for NRR. Noble metals, such as Pt, Re, Rh, and Ir, are at the top of the HER volcano plot, because they bind hydrogen with just the perfect strength to effectively catalyze the reduction of protons or water to H_2 . On the right leg of the HER volcano are catalysts such as Ta, Ti, and Mo, which bind hydrogen very strongly, and consequently, the exchange currents are lower as additional work needs to be used to desorb the H from the metal surface as H_2 . On the left side of the volcano in Figure 5A decent HER promoters are present (Ni, Fe, Co, Cu, and Au). Fe is at the same time a good catalyst for both NRR (Figure 4) and for HER (Figure 5A). This is an advantage in Haber-Bosch process, where the catalyst has to be good in binding both reactants, whereas this is a drawback in electrochemical NRR, because at reducing conditions and in aqueous electrolytes, Fe will be completely covered by H adatoms (Skúlason et al., 2012).

On the left leg of the HER volcano (Figure 5A) predominantly post-transition metals are found (Bi, Ga, In), which poorly bind H and are poor promoters of HER. Ga and In are also close to the top of the NRR volcano plot (Figure 4), which makes them promising candidates for NRR. Mn and Cr are not plotted on Figure 5A because MH bond energy data were not available. Mn and Cr HER exchange currents are very low, 1.25×10^{-11} and $1.25 \times 10^{-7} \text{ A cm}^{-2}$ for Mn and Cr (Trasatti, 1972), respectively, and are equally as good candidates for NRR as Ga and In (Figure 4).

The rates of electrochemical NRR are pH dependent, as they involve a series of PCET steps (Figure 1). In general, at pH 0 NRR rates are the highest, whereas at pH 14 the NRR rates are the lowest because of the lack of protons in the solution. Similarly, at pH 0 HER occurs at very high rates as it involves direct reduction of protons at the electrode surface (Volmer step), and then either H reaction with another H (Tafel step) or with another H^+ and e^- (Heyrovsky step) to form H_2 . At higher pH, the kinetics of HER become sluggish and exchange currents lower, because the first step is water dissociation, followed by Tafel or Heyrovsky steps (Subbaraman et al., 2011). This means at higher pH, higher applied potential is needed to start the onset of HER. This all translates to the fact that at low pH, NRR rates can be expected high but NRR selectivity low as HER kinetics are supreme, whereas at higher pH, NRR rates are low but NRR has a chance to prevail as the kinetics of HER are sluggish. The charge-transfer coefficient (α) of HER is pH dependent (Haghighat and Dawlaty, 2016); it falls from close to ideal values of 0.6–0.4 at pH 0 to about 0.2 at pH 4

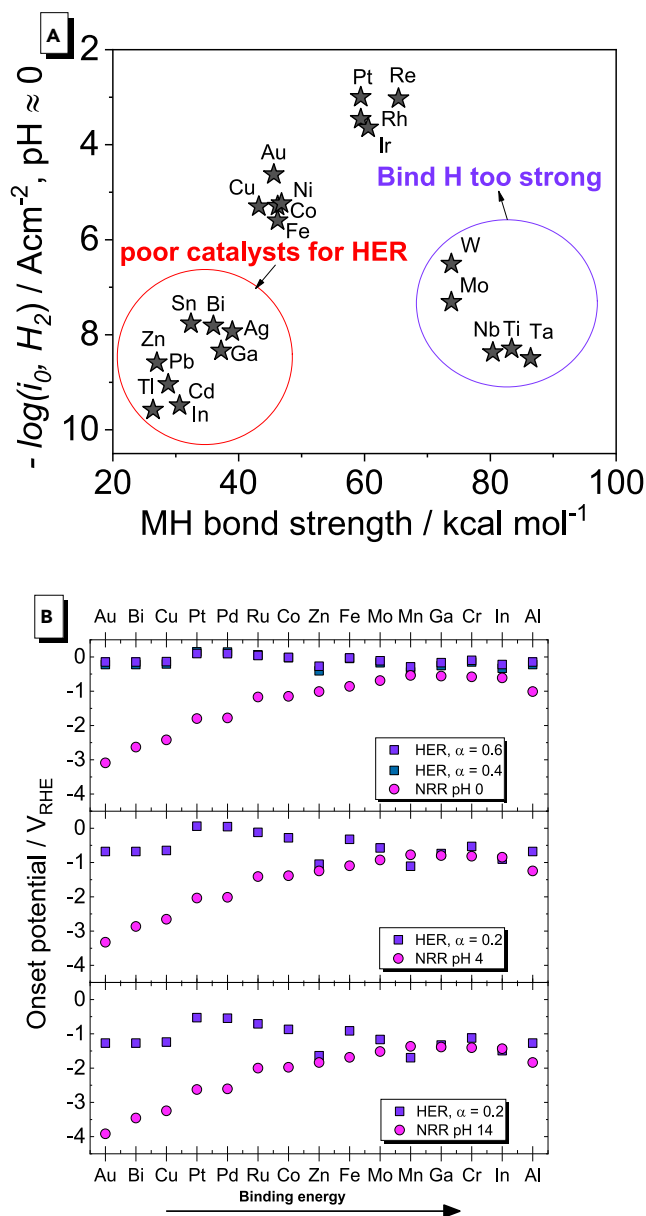


Figure 5. NRR over HER Selectivity Plot at pH 0, 4, and 14

(A) Volcano plot of HER. Experimental exchange currents of HER versus MH bond strengths (heat of adsorption of H₂ gas) for different metals (M), where the data are taken from [Trasatti \(1972\)](#).

(B) Potentials needed to start the onset of HER and NRR at pH 0, 4, and 14 are calculated as explained in the [Transparent Methods](#) section. Black arrow shows in which direction N-binding energy (E_{cell} (MN)) increases.

and is nearly constant at pH > 4 (see [Transparent Methods](#) for more details). In general, at pH 4 the kinetics of HER will experience a breaking point and start to be sluggish, with no change all the way up to pH 14. This is the reasoning behind choosing pH 0 (supreme HER rates, high NRR rates), 4 (moderate NRR rates, low to moderate HER rates), and 14 (low NRR rates, low to moderate HER rates) in the following discussion.

In [Figure 5B](#) we compare the onset potentials at which HER and NRR will occur at pH 0, 4, and 14 on different metal catalysts. A more detailed insight in the data in [Figure 5B](#) can be found in [Supplemental Information](#) and [Table S3](#). We note again that onset potentials calculated by DFT agree well with experimentally measured onset potentials ([Nørskov et al., 2004, 2005](#); [Greeley et al., 2006, 2009](#); [Skúlason et al., 2010](#), [Skúlason et al., 2012](#); [Gislason and Skúlason, 2019](#); [Montoya et al., 2015](#); [Kuhl et al., 2014](#); [Peterson et al., 2010](#); [Peterson and Nørskov, 2012](#); [Hussain](#)

et al., 2018). With respect to HER onset potentials used, we estimate the minimum applied potential needed to evolve H_2 at a rate of $1 \times 10^{-5} \text{ A cm}^{-2}$. This is a low-end of reported rates (current density) at which ammonia evolves on metal catalysts (Andersen et al., 2019). We note that we have used exchange current density measured at pH 0 to calculate the HER potentials at higher pH (see the [Transparent Methods](#) and [Table S3 in Supplemental Information](#)), and thus we have underestimated the HER onset potential at higher pH.

Figure 5B clearly shows that at pH 0, all metals, even the poor HER promoters such as Mn, Ga, and In, require less negative onset potentials (less work) to start HER than NRR. At higher pH, only Mn and In need lower applied potentials to start NRR than HER. Ga appears to be on the edge, as NRR and HER onset potentials are close. It might also be that Ga needs lower applied potential to start NRR than HER, as we have underestimated the applied potential needed to start the onset of HER (it is probably more negative). Considering Ru (Andersen et al., 2019), Au (Tan et al., 2019), Bi (Hao et al., 2019), Pd (Wang et al., 2018), and Cu (Lin et al., 2019), for which electrochemical NRR was reported in aqueous media, and some with high FE at even positive potentials, this does not appear possible at any pH, a statement corroborated by Figure 5B. Considering Ru, the latest credible work following rigorous protocol reported FE around 0.001% at pH 13 and the measured ammonia concentration was below the detection limit, which agrees very well with Figure 5B where we do not expect to have any NRR selectivity in water on Ru (Andersen et al., 2019). In the case of Fe, which is the most investigated catalyst in NRR, Figure 5B shows that at all pH, the onset potential for HER is more positive than for NRR. However, some experimental studies with Fe-based catalysts report 35%–60% FE at pH 7–14 (Licht et al., 2014; Zhou et al., 2017; Wang et al., 2019). One of them (35% FE) uses Fe_2O_3 in molten salt at higher temperatures using steam as a proton source (Licht et al., 2014). This study has recently been retracted, because nitrates impurities in the catalyst were reduced instead of N_2 (Licht et al., 2020). Another study performed NRR in ionic liquid at very low H_2O concentration (ppm levels), and there ionic liquid had a beneficial effect on selectivity of NRR (Zhou et al., 2017). Overall, there are a large number of false-positive measurements in the literature, and thus many studies that report high FE at not sufficiently negative potentials in aqueous media, and are in contradiction with Figure 5B, should be taken with a great level of precaution.

Thermodynamic Stability of the Most Promising Metal Catalysts in Water

Here, we take into consideration the thermodynamic stability of Mn, Ga, and In in water (see the Pourbaix diagrams in [Supplemental Information](#)). None of the metals are thermodynamically stable in water, and depending on the pH and whether oxygen is present in water, these metals will be oxidized by water and/or oxygen and corrode either to metal ions or oxides. However, the metals will be used as cathodes in water at reducing conditions, and in this sense, they will have a “cathodic anticorrosive” protection. If the applied potential on the cathode is negative enough, these metals will not corrode in water. In case of the most reactive metal, Mn, we have identified that at pH 14 and the applied potential of $-1.65 V_{RHE}$, its metal surface will remain intact and free of oxides. HER will not occur and $-1.65 V_{RHE}$ is more than negative enough to promote NRR (see [Supplemental Information](#) and [Figure S1](#)). In case of Ga, we have identified that at pH 4, and the applied potential of $-0.8 V_{RHE}$, Ga will be thermodynamically stable in water and NRR will occur as well as HER ([Supplemental Information](#) and [Figure S2](#)). Finally, at pH 4 and $-0.85 V_{RHE}$, and pH 14 and $-1.21 V_{RHE}$, In will be free of oxides and thermodynamically stable in water; the potential applied will be negative enough to promote NRR, but HER will not occur ([Supplemental Information](#) and [Figure S3](#)). We stress out here that Mn, Ga, and In are also highly promising candidates for NRR in non-aqueous media, an emerging research area, where their thermodynamic stability will not be challenged by the presence of water. They bind nitrogen similarly well as Li, but (1) the applied potential does not have to be nearly as negative as it is in case of Li where NH_3 was synthesized at around $-3.8 V_{RHE}$ (potentials needed to start NRR on Mn, Ga, and In are -0.54 , -0.56 , and $-0.61 V_{RHE}$, respectively) (Schwalbe et al., 2020) and (2) they are not nearly as reactive with solvents as Li. The candidates we propose here remain to be experimentally verified, which is out of the scope of the present study.

In conclusion, we have performed perhaps the most extensive screening study of possible catalysts for NRR where we placed 31 different elements from s-, p-, d-, lanthanides, and actinides block on the same volcano plot, and this presents to date the largest volcano plot for NRR. We found that the most investigated catalysts so far Fe, Bi, Au, Pd, Mo, Ru, and Cu cannot selectively catalyze electrochemical NRR in water. They need a smaller applied potential to start the onset of HER than NRR in aqueous media at room temperature and any pH. Nevertheless, some of them (Bi, Au, Pd, and Cu) are touted in the literature as selective in electrochemical synthesis of ammonia in aqueous media. Based on our data we feel the urge to raise a valid concern about if electrochemical NRR in water has been even demonstrated so far (above 0.001% FE) and whether the earlier works reported reduction of, e.g. NO_x or nitrates while even not being aware of that.

Nevertheless, we identified new possible NRR catalysts, which all are poor HER promoters and good N binders, Mn, Ga, and In. Mn is an earth-abundant element that we find the most reactive (lowest limiting potential) and selective. We have identified conditions at which these metals remain thermodynamically stable in water and catalyze NRR selectively over HER in aqueous media. In addition, we strongly believe that these metals present to date the most reasonable choice for NRR in non-aqueous media. The last but not the least important finding of this study is that we have observed a large gap, at the top of the volcano plot, where unidentified elements lie. Mo, Fe, or the new overlooked catalysts we found are not at the top of the volcano plot, but unidentified elements are. We believe the unidentified elements do exist in the periodic system of elements and we hope our future research efforts will lead to their discovery, as well as this work will inspire other researchers in the field to do so.

Limitations of the Study

Lead Contact

Further information and requests should be directed to and will be fulfilled by the Lead Contact, Emil Dražević (edrazevic@eng.au.dk).

Materials Availability

The study did not generate new unique reagents or there are restrictions.

Data and Code Availability

The study does not use any unpublished custom code, software, or algorithm that is central to supporting the main claims of the paper.

METHODS

All methods can be found in the accompanying [Transparent Methods supplemental file](#).

SUPPLEMENTAL INFORMATION

Supplemental Information can be found online at <https://doi.org/10.1016/j.isci.2020.101803>.

ACKNOWLEDGMENTS

We acknowledge anonymous reviewers for very constructive feedbacks, which led to a considerable improvement of the present study. There was no funding supporting this study.

AUTHOR CONTRIBUTIONS

Conceptualization, E.D.; Methodology, E.D. and E.S.; Formal Analysis, E.D.; Investigation, E.D.; Resources, E.D.; Writing – Original Draft, E.D.; Writing – Review & Editing, E.S. and E.D.; Visualization, E.D. and E.S.

DECLARATION OF INTERESTS

The authors declare no competing interests.

Received: July 6, 2020

Revised: August 18, 2020

Accepted: November 9, 2020

Published: December 18, 2020

REFERENCES

Abghoui, Y., Garden, A.L., Hlynsson, V.F., Björgvinsdóttir, S., Ólafsdóttir, H., and Skúlason, E. (2015). Enabling electrochemical reduction of nitrogen to ammonia at ambient conditions through rational catalyst design. *Phys. Chem. Chem. Phys.* 17, 4909–4918.

Abghoui, Y., Sigtryggsson, S.B., and Skúlason, E. (2019). Biomimetic nitrogen fixation catalyzed by transition metal sulfide

surfaces in an electrolytic cell. *ChemSusChem* 12, 4265–4273.

Abild-Pedersen, F., Greeley, J., Studt, F., Rossmeisl, J., Munter, T.R., Moses, P.G., Skúlason, E., Bligaard, T., and Nørskov, J.K. (2007). Scaling properties of adsorption energies for hydrogen-containing molecules on transition-metal surfaces. *Phys. Rev. Lett.* 99, 016105.

Akira, T., Akihiko, K., and Tadayoshi, S. (1993). Efficient electrochemical reduction of N₂ to NH₃ catalyzed by lithium. *Chem. Lett.* 22, 851–854.

Andersen, S.Z., Čolić, V., Yang, S., Schwalbe, J.A., Nielander, A.C., Mccanney, J.M., Enemark-Rasmussen, K., Baker, J.G., Singh, A.R., Rohr, B.A., et al. (2019). A rigorous electrochemical ammonia synthesis protocol with quantitative isotope measurements. *Nature* 570, 504–508.

- Appl, M. (2011). Ammonia, 2. Production processes, Ullmann's Encyclopedia of Industrial Chemistry. https://doi.org/10.1002/14356007.o02_o11.
- Bruckard, W.J., and Woodcock, J.T. (2007). Characterisation and treatment of Australian salt cakes by aqueous leaching. *Minerals Eng.* 20, 1376–1390.
- Chen, S., Perathoner, S., Ampelli, C., Mebrahtu, C., Su, D., and Centi, G. (2017). Electro-catalytic synthesis of ammonia at room temperature and atmospheric pressure from water and nitrogen on a carbon-nanotube-based electrocatalyst. *Angew. Chem. Int. Ed.* 56, 2699–2703.
- Choi, J., Du, H.-L., Nguyen, C.K., Suryanto, B.H.R., Simonov, A.N., and Macfarlane, D.R. (2020). Electroreduction of nitrates, nitrites and gaseous nitrogen oxides: a potential source of ammonia in dinitrogen reduction (NRR) studies. *ACS Energy Lett.* 5, 2095–2097.
- Comer, B.M., Fuentes, P., Dimkpa, C.O., Liu, Y.-H., Fernandez, C.A., Arora, P., Realf, M., Singh, U., Hatzell, M.C., and Medford, A.J. (2019). Prospects and challenges for solar fertilizers. *Joule* 3, 1578–1605.
- Deng, J., Iñiguez, J.A., and Liu, C. (2018). Electrocatalytic nitrogen reduction at low temperature. *Joule* 2, 846–856.
- Foster, S.L., Bakovic, S.I.P., Duda, R.D., Maheshwari, S., Milton, R.D., Minteer, S.D., Janik, M.J., Renner, J.N., and Greenlee, L.F. (2018). Catalysts for nitrogen reduction to ammonia. *Nat. Catal.* 1, 490–500.
- Giddey, S., Badwal, S.P.S., and Kulkarni, A. (2013). Review of electrochemical ammonia production technologies and materials. *Int. J. Hydrogen Energy* 38, 14576–14594.
- Gíslason, P.M., and Skúlason, E. (2019). Catalytic trends of nitrogen doped carbon nanotubes for oxygen reduction reaction. *Nanoscale* 11, 18683–18690.
- Greeley, J., Jaramillo, T.F., Bonde, J., Chorkendorff, I., and Nørskov, J.K. (2006). Computational high-throughput screening of electrocatalytic materials for hydrogen evolution. *Nat. Mater.* 5, 909–913.
- Greeley, J., Stephens, I.E.L., Bondarenko, A.S., Johansson, T.P., Hansen, H.A., Jaramillo, T.F., Rossmeisl, J., Chorkendorff, I., and Nørskov, J.K. (2009). Alloys of platinum and early transition metals as oxygen reduction electrocatalysts. *Nat. Chem.* 1, 552–556.
- Greenlee, L.F., Renner, J.N., and Foster, S.L. (2018). The use of controls for consistent and accurate measurements of electrocatalytic ammonia synthesis from dinitrogen. *ACS Catal.* 8, 7820–7827.
- Greenwood, N.N., and Earnshaw, A. (1997). 11-nitrogen. In *Chemistry of the Elements*, Second Edition, N.N. Greenwood and A. Earnshaw, eds. (Butterworth-Heinemann), pp. 407–471.
- Guo, W., Liang, Z., Zhao, J., Zhu, B., Cai, K., Zou, R., and Xu, Q. (2018b). Hierarchical cobalt phosphide hollow nanocages toward electrocatalytic ammonia synthesis under ambient pressure and room temperature. *Small Methods* 2, 1800204.
- Guo, C., Ran, J., Vasileff, A., and Qiao, S.-Z. (2018a). Rational design of electrocatalysts and photo(electro)catalysts for nitrogen reduction to ammonia (NH₃) under ambient conditions. *Energy Environ. Sci.* 11, 45–56.
- Haghighat, S., and Dawlaty, J.M. (2016). pH dependence of the electron-transfer coefficient: comparing a model to experiment for hydrogen evolution reaction. *The J. Phys. Chem. C* 120, 28489–28496.
- Han, N., Ding, P., He, L., Li, Y., and Li, Y. (2020). Promises of main group metal-based nanostructured materials for electrochemical CO₂ reduction to formate. *Adv. Energy Mater.* 10, 1902338.
- Hanifpour, F., Sveinbjörnson, A., Canales, C.P., Skúlason, E., and Flosadóttir, H.D. (2020). Preparation of Nafion® membranes for reproducible ammonia quantification in nitrogen reduction reaction experiments. *Angew. Chem. Int. Ed.* 59, 1–6.
- Hao, Y.-C., Guo, Y., Chen, L.-W., Shu, M., Wang, X.-Y., Bu, T.-A., Gao, W.-Y., Zhang, N., Su, X., Feng, X., et al. (2019). Promoting nitrogen electroreduction to ammonia with bismuth nanocrystals and potassium cations in water. *Nat. Catal.* 2, 448–456.
- Hoshyargar, F., Khan, H., Kalantar-Zadeh, K., and O'mullane, A.P. (2015). Generation of catalytically active materials from a liquid metal precursor. *Chem. Commun.* 51, 14026–14029.
- Hussain, J., Jónsson, H., and Skúlason, E. (2018). Calculations of product selectivity in electrochemical CO₂ reduction. *ACS Catal.* 8, 5240–5249.
- Kepp, K.P. (2018). Accuracy of theoretical catalysis from a model of iron-catalyzed ammonia synthesis. *Commun. Chem.* 1, 63.
- Kuhl, K.P., Hatsukade, T., Cave, E.R., Abram, D.N., Kibsgaard, J., and Jaramillo, T.F. (2014). Electrocatalytic conversion of carbon dioxide to methane and methanol on transition metal surfaces. *J. Am. Chem. Soc.* 136, 14107–14113.
- Kyriakou, V., Garagounis, I., Vasileiou, E., Vourros, A., and Stoukides, M. (2017). Progress in the electrochemical synthesis of ammonia. *Catal. Today* 286, 2–13.
- Kyriakou, V., Garagounis, I., Vourros, A., Vasileiou, E., and Stoukides, M. (2020). An electrochemical haber-bosch process. *Joule* 4, 142–158.
- Licht, S., Cui, B., Wang, B., Li, F.-F., Lau, J., and Liu, S. (2014). Ammonia synthesis by N₂ and steam electrolysis in molten hydroxide suspensions of nanoscale Fe₂O₃. *Science* 345, 637.
- Licht, S., Cui, B., Wang, B., Li, F.-F., Lau, J., and Liu, S. (2020). Retraction. *Science* 369, 780.
- Lin, Y.-X., Zhang, S.-N., Xue, Z.-H., Zhang, J.-J., Su, H., Zhao, T.-J., Zhai, G.-Y., Li, X.-H., Antonietti, M., and Chen, J.-S. (2019). Boosting selective nitrogen reduction to ammonia on electron-deficient copper nanoparticles. *Nat. Commun.* 10, 4380.
- Macfarlane, D.R., Cherepanov, P.V., Choi, J., Suryanto, B.H.R., Hodgetts, R.Y., Bakker, J.M., Ferrero Vallana, F.M., and Simonov, A.N. (2020). A roadmap to the ammonia economy. *Joule* 4, 1186–1205.
- Mcenaney, J.M., Singh, A.R., Schwalbe, J.A., Kibsgaard, J., Lin, J.C., Cargnello, M., Jaramillo, T.F., and Nørskov, J.K. (2017). Ammonia synthesis from N₂ and H₂O using a lithium cycling electrification strategy at atmospheric pressure. *Energy Environ. Sci.* 10, 1621–1630.
- Montoya, J.H., Tsai, C., Vojvodic, A., and Nørskov, J.K. (2015). The challenge of electrochemical ammonia synthesis: a new perspective on the role of nitrogen scaling relations. *ChemSusChem* 8, 2180–2186.
- Nørskov, J.K., Bligaard, T., Logadottir, A., Kitchin, J.R., Chen, J.G., Pandelov, S., and Stimming, U. (2005). Trends in the exchange current for hydrogen evolution. *J. Electrochem. Soc.* 152, J23.
- Nørskov, J.K., Rossmeisl, J., Logadottir, A., Lindqvist, L., Kitchin, J.R., Bligaard, T., and Jónsson, H. (2004). Origin of the overpotential for oxygen reduction at a fuel-cell cathode. *J. Phys. Chem. B* 108, 17886–17892.
- Peterson, A.A., Abild-Pedersen, F., Studt, F., Rossmeisl, J., and Nørskov, J.K. (2010). How copper catalyzes the electroreduction of carbon dioxide into hydrocarbon fuels. *Energy Environ. Sci.* 3, 1311–1315.
- Peterson, A.A., and Nørskov, J.K. (2012). Activity descriptors for CO₂ electroreduction to methane on transition-metal catalysts. *J. Phys. Chem. Lett.* 3, 251–258.
- Reller, C., Schmid, B., Schmid, G. & Taroata, D. 2018. High-current Process for the Production of Ammonia Germany Patent Application.
- Rouwenhorst, K.H.R., van der Ham, A.G.J., Mul, G., and Kersten, S.R.A. (2019). Islanded ammonia power systems: technology review & conceptual process design. *Renew. Sustain. Energy Rev.* 114, 109339.
- Schwalbe, J.A., Statt, M.J., Chosy, C., Singh, A.R., Rohr, B.A., Nielander, A.C., Andersen, S.Z., Mcenaney, J.M., Baker, J.G., Jaramillo, T.F., et al. (2020). A combined theory-experiment analysis of the surface species in lithium-mediated NH₃ electrosynthesis. *ChemElectroChem* 7, 1542–1549.
- Singh, A.R., Rohr, B.A., Schwalbe, J.A., Cargnello, M., Chan, K., Jaramillo, T.F., Chorkendorff, I., and Nørskov, J.K. (2017). Electrochemical ammonia synthesis—the selectivity challenge. *ACS Catal.* 7, 706–709.
- Singh, A.R., Rohr, B.A., Statt, M.J., Schwalbe, J.A., Cargnello, M., and Nørskov, J.K. (2019). Strategies toward selective electrochemical ammonia synthesis. *ACS Catal.* 9, 8316–8324.
- Skúlason, E., Bligaard, T., Gudmundsdóttir, S., Studt, F., Rossmeisl, J., Abild-Pedersen, F., Vegge, T., Jónsson, H., and Nørskov, J.K. (2012). A theoretical evaluation of possible transition metal electro-catalysts for N₂ reduction. *Phys. Chem. Chem. Phys.* 14, 1235–1245.
- Skúlason, E., Tripkovic, V., Björketun, M.E., Gudmundsdóttir, S., Karlberg, G., Rossmeisl, J.,

Bligaard, T., Jónsson, H., and Nørskov, J.K. (2010). Modeling the electrochemical hydrogen oxidation and evolution reactions on the basis of density functional theory calculations. *J. Phys. Chem. C* *114*, 18182–18197.

Subbaraman, R., Tripkovic, D., Strmcnik, D., Chang, K.-C., Uchimura, M., Paulikas, A.P., Stamenkovic, V., and Markovic, N.M. (2011). Enhancing hydrogen evolution activity in water splitting by tailoring Li+-Ni(OH)2<-Pt interfaces. *Science* *334*, 1256–1260.

Suryanto, B.H.R., Du, H.-L., Wang, D., Chen, J., Simonov, A.N., and Macfarlane, D.R. (2019). Challenges and prospects in the catalysis of electroreduction of nitrogen to ammonia. *Nat. Catal.* *2*, 290–296.

Tan, L., Yang, N., Huang, X., Peng, L., Tong, C., Deng, M., Tang, X., Li, L., Liao, Q., and Wei, Z.

(2019). Synthesis of ammonia via electrochemical nitrogen reduction on high-index faceted Au nanoparticles with a high faradaic efficiency. *Chem. Commun.* *55*, 14482–14485.

Tang, C., and Qiao, S.-Z. (2019). How to explore ambient electrocatalytic nitrogen reduction reliably and insightfully. *Chem. Soc. Rev.* *48*, 3166–3180.

Tayyebi, E., Abghoui, Y., and Skúlason, E. (2019). Elucidating the mechanism of electrochemical N₂ reduction at the Ru(0001) electrode. *ACS Catal.* *9*, 11137–11145.

Trasatti, S. (1972). Work function, electronegativity, and electrochemical behaviour of metals: III. Electrolytic hydrogen evolution in acid solutions. *J. Electroanal. Chem. Interf. Electrochem.* *39*, 163–184.

Wang, J., Yu, L., Hu, L., Chen, G., Xin, H., and Feng, X. (2018). Ambient ammonia synthesis via palladium-catalyzed electrohydrogenation of dinitrogen at low overpotential. *Nat. Commun.* *9*, 1795.

Wang, M., Liu, S., Qian, T., Liu, J., Zhou, J., Ji, H., Xiong, J., Zhong, J., and Yan, C. (2019). Over 56.55% Faradaic efficiency of ambient ammonia synthesis enabled by positively shifting the reaction potential. *Nat. Commun.* *10*, 341.

Zhou, F., Azofra, L.M., Ali, M., Kar, M., Simonov, A.N., McDonnell-Worth, C., Sun, C., Zhang, X., and Macfarlane, D.R. (2017). Electro-synthesis of ammonia from nitrogen at ambient temperature and pressure in ionic liquids. *Energy Environ. Sci.* *10*, 2516–2520.

iScience, Volume 23

Supplemental Information

Are There Any Overlooked Catalysts for Electrochemical NH₃ Synthesis—New Insights from Analysis of Thermochemical Data

Emil Dražević and Egill Skúlason

Supplemental Information

Contents

SUPPLEMENTAL DATA ITEMS	2
S1.1 Definitions and notations of key terms used in this work	2
S1.2 Thermochemical data	3
S1.3 MN formation reactions	5
S1.4 MN to NH ₃ and M formation reactions	7
S1.5 Data for large volcano plot	9
S1.6 Potentials needed to start onset for NRR and HER at different pH	10
S1.7 POURBAIX diagrams of Mn, Ga and In.....	12
TRANSPARENT METHODS.....	15
SUPPLEMENTAL REFERENCES.....	18

SUPPLEMENTAL DATA ITEMS

S1.1 Definitions and notations of key terms used in this work

- The definitions and notations are related to Figures 1, 2, 3, 4 and 5 in the main text.

Limiting potential (U_L): The potential vs. the reversible hydrogen electrode (RHE) for a given reaction step in e.g. NRR.

Equilibrium potential: The potential when reactants and products are in equilibrium. In the case of HER it is defined as 0 V_{RHE} at pH 0 and standard conditions ($T = 298.15$ K and 1 bar pressure). In the case of NRR it is +0.0566 V_{RHE} at pH 0 and standard conditions.

Overpotential: The difference between the limiting potential of the potential determining step (PDS) and the equilibrium potential.

Onset potential: The potential vs. RHE needed to start the onset of a chemical reaction (e.g. HER or NRR). See the Experimental section for more details.

E_{cell} : Cell potentials defined and calculated as explained in the Experimental section.

Potential determining step (PDS): The most endergonic reaction step of an electrochemical reaction. This reaction step determines or limits the potential needed to start the onset of the electrochemical reaction.

Proton coupled electron transfer (PCET): A heterogeneous catalytic electrochemical reaction step where proton transfer and electron transfer are coupled and take place simultaneously.

Faradaic efficiency (FE): The partial current density towards a given product (e.g. NH_3) divided with the total current flowing through the cell.

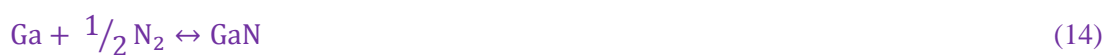
S1.2 Thermochemical data

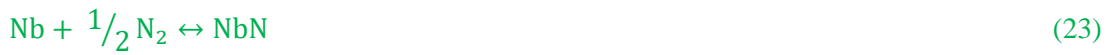
Table S1. Related to Fig 2. Thermochemical data used to calculate cell potentials in the Transparent methods section. The thermochemical data were taken from references (Pankratz et al., 1984, Lide, 2009).

Compound	$\Delta H/\text{kJ mol}^{-1}$	$S(298\text{K})/\text{J mol}^{-1} \text{K}^{-1}$
AlN	-316.3	20.1
Ba ₃ N ₂	-363.1	152.3
BN	-254.4	15.1
Be ₃ N ₂	-588.3	34.4
Ca ₃ N ₂	-430.1	104.6
CeN	-326.4	44.4
Co ₃ N	8.4	98.7
Cr ₂ N	-125.5	64.9
CrN	-117.1	37.7
ErN	-357.7	77.4
Fe ₂ N	-3.76	101.3
Fe ₄ N	-10.5	154.8
HoN	-336.8	79.5
GaN	-110.5	36.5
InN	-138.0	43.5
HfN	-373.6	48.
LaN	-303.3	44.4
Li ₃ N	-164.6	87.9
Mg ₃ N ₂	-460.7	62.6
Mn ₄ N	-128.7	142.9
Mn ₅ N ₂	-204.2	187.4
MoN _{0.5}	-40.8	31.6
NbN	-235.1	34.5
Nb ₂ N	-250.6	79.5
ScN	-313.8	29.7
Si ₃ N ₄	-743.5	112.9
SmN	-322.2	73.6
Sr ₃ N ₂	-391.2	134.7
ThN	-391.2	56.0
TaN	-251.5	42.7
Ta ₂ N	-271.5	86.1
VN _{0.465}	-133.0	26.7
VN	-217.0	37.3
YbN	-363.6	66.9
Zn ₃ N ₂	-22.6	108.8
ZrN	-364.8	38.9
Al	0	28.3
Ba	0	62.5
B	0	5.9

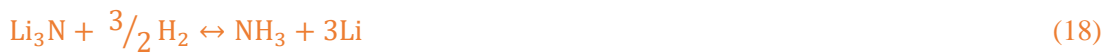
Be	0	9.5
Ca	0	41.6
Ce	0	72.0
Co	0	30.0
Cr	0	23.8
Er	0	73.2
Fe	0	27.3
Ho	0	75.3
Ga	0	40.8
In	0	57.8
Hf	0	43.6
La	0	56.9
Li	0	29.12
Mg	0	32.67
Mn	0	32.0
Mo	0	28.7
Nb	0	36.4
Sc	0	34.6
Si	0	18.8
Sm	0	69.6
Sr	0	55.0
Th	0	51.8
Ta	0	41.5
V	0	28.9
Yb	0	59.9
Zn	0	41.6
Zr	0	39.0
H ₂	0	130.7
NH ₃	-45.898	192.7

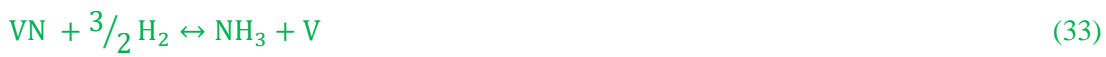
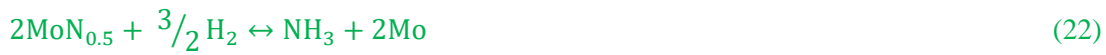
S1.3 MN formation reactions – Related to Fig 2 and 3. Color codes: purple-posttransition metals, orange-s-block metals, green- transition metals and black- lanthanides, actinides, B and Si from p-block.





S1.4 MN to NH₃ and M formation reactions – Related to Fig 2 and 3. Color codes: purple-posttransition metals, orange- s-block metals, green- transition metals and black- lanthanides, actinides, B and Si from p-block.





S1.5 Data for large volcano plot

Table S2. Related to Figure 3, 4 and 5. A more detailed representation of the parameters calculated in this study. Color codes: purple-posttransition metals, orange- s-block metals, green- transition metals and black-lanthanides, actinides, B and Si from p-block. E_{cell} (MN) and E_{cell} (MN to NH₃) are calculated as explained in the S2 section. U_L below for 1st and 5th PCET are calculated using linear relations obtained from Fig 3A and E_{cell} (MN).

Element	E_{cell} (MN)/V	E_{cell} (MN to NH ₃)/V	U_L (1 st) / V _{RHE}	U_L (5 th) / V _{RHE}
Al	0.99	-0.93	1.91	-1.01
Ba	0.51	-0.45	0.59	-0.70
B	0.86	-0.73	1.57	-0.93
Be	0.89	-0.86	1.65	-0.95
Ca	0.64	-0.58	0.94	-0.78
Ce	1.00	-0.94	1.95	-1.02
Co	-0.12	0.18	-1.15	-0.29
Cr	0.35	-0.30	0.16	-0.60
Cr	0.32	-0.26	0.07	-0.58
Er	1.14	-1.08	2.34	-1.11
Fe	-0.04	0.09	-0.92	-0.35
Fe	-0.02	0.07	-0.86	-0.36
Ho	1.07	-1.01	2.14	-1.07
Ga	0.29	-0.22	-0.02	-0.56
In	0.36	-0.31	0.19	-0.61
Hf	1.20	-1.14	2.50	-1.15
La	0.94	-0.88	1.77	-0.98
Li	0.44	-0.41	0.41	-0.66
Mg	0.69	-0.62	1.10	-0.82
Mn	0.36	-0.30	0.18	-0.60
Mn	0.27	-0.21	-0.08	-0.54
Mo	0.05	0.04	-0.69	-0.40
Nb	0.71	-0.66	1.15	-0.83
Nb	0.77	-0.72	1.32	-0.87
Sc	0.98	-0.92	1.90	-1.01
Si	0.56	-0.50	0.73	-0.73
Sm	1.02	-0.96	2.00	-1.03
Sr	0.57	-0.50	0.75	-0.74
Ta	0.77	-0.71	1.32	-0.87
Ta	0.84	-0.79	1.51	-0.92
Th	1.25	-1.33	0.42	-1.19
V	0.88	-0.19	1.63	-0.95
V	0.41	-0.57	0.32	-0.64
Yb	1.16	-1.13	2.41	-1.13
Zn	-0.07	0.12	-1.01	-0.33
Zr	1.16	-1.11	2.40	-1.13

S1.6 Potentials to start onset for NRR and HER at different pH

Table S3. Related to Figure 5. Parameters used to calculate values presented in Figure 5B, as described in the section Transparent methods. Underlined and bolded are the elements where more positive potentials are needed to start the onset of NRR than HER. Ga is underlined and italic, to show that the values are very close to each other.

Parameters for Butler-Volmer equation				Onset potential, pH = 0, / V			Onset potential, pH = 4, / V _{RHE}		Onset potential, pH = 14 / V _{RHE}	
Element	log <i>j</i> _o / A cm ⁻²	<i>j</i> _c /A cm ⁻²	<i>j</i> _o / A cm ⁻²	NRR	HER. α = 0.4	HER. α = 0.6	HER. α = 0.2	NRR (pH)	HER. α = 0.2	NRR (pH)
Co	-5.3	1.00E-05	5.01E-06	-1.15	-0.02	-0.01	-0.28	-1.39	-0.87	-1.98
Zn	-10.5	1.00E-05	3.16E-11	-1.01	-0.41	-0.27	-1.05	-1.25	-1.64	-1.84
Fe	-5.6	1.00E-05	2.51E-06	-0.86	-0.04	-0.03	-0.32	-1.10	-0.91	-1.69
Mo	-7.3	1.00E-05	5.01E-08	-0.69	-0.17	-0.11	-0.58	-0.93	-1.17	-1.52
Mn	-10.9	1.00E-05	1.26E-11	-0.54	-0.44	-0.29	<u>-1.11</u>	<u>-0.78</u>	<u>-1.70</u>	<u>-1.37</u>
Ga	-8.4	1.00E-05	3.98E-09	-0.56	-0.25	-0.17	<u>-0.74</u>	<u>-0.80</u>	<u>-1.33</u>	<u>-1.39</u>
Cr	-7.0	1.00E-05	1.00E-07	-0.58	-0.15	-0.10	-0.53	-0.82	-1.12	-1.41
In	-9.5	1.00E-05	3.16E-10	-0.61	-0.33	-0.22	<u>-0.90</u>	<u>-0.85</u>	<u>-1.49</u>	<u>-1.44</u>
Al	-8.0	1.00E-05	1.00E-08	-1.01	-0.22	-0.15	-0.68	-1.25	-1.27	-1.84
Au	-8.0	1.00E-05	1.00E-08	-3.09	-0.22	-0.15	-0.68	-3.33	-1.27	-3.92
Bi	-8.0	1.00E-05	1.00E-08	-2.63	-0.22	-0.15	-0.68	-2.87	-1.27	-3.46
Cu	-7.8	1.00E-05	1.58E-08	-2.42	-0.21	-0.14	-0.65	-2.66	-1.24	-3.25
Pt	-3.0	1.00E-05	1.00E-03	-1.80	0.15	0.10	0.06	-2.04	-0.53	-2.63
Pd	-3.1	1.00E-05	7.94E-04	-1.78	0.14	0.09	0.04	-2.02	-0.55	-2.61
Ru	-4.1	1.00E-05	6.31E-05	-1.17	0.06	0.04	-0.12	-1.41	-0.71	-2-.00

S1.7 POURBAIX diagrams of Mn, Ga and In

Related to Figure 5 and the part of the discussion titled **Thermodynamic stability of the most promising metal catalysts in water**. Pourbaix diagrams were built on a website materialsproject.org (Jain et al., 2013).

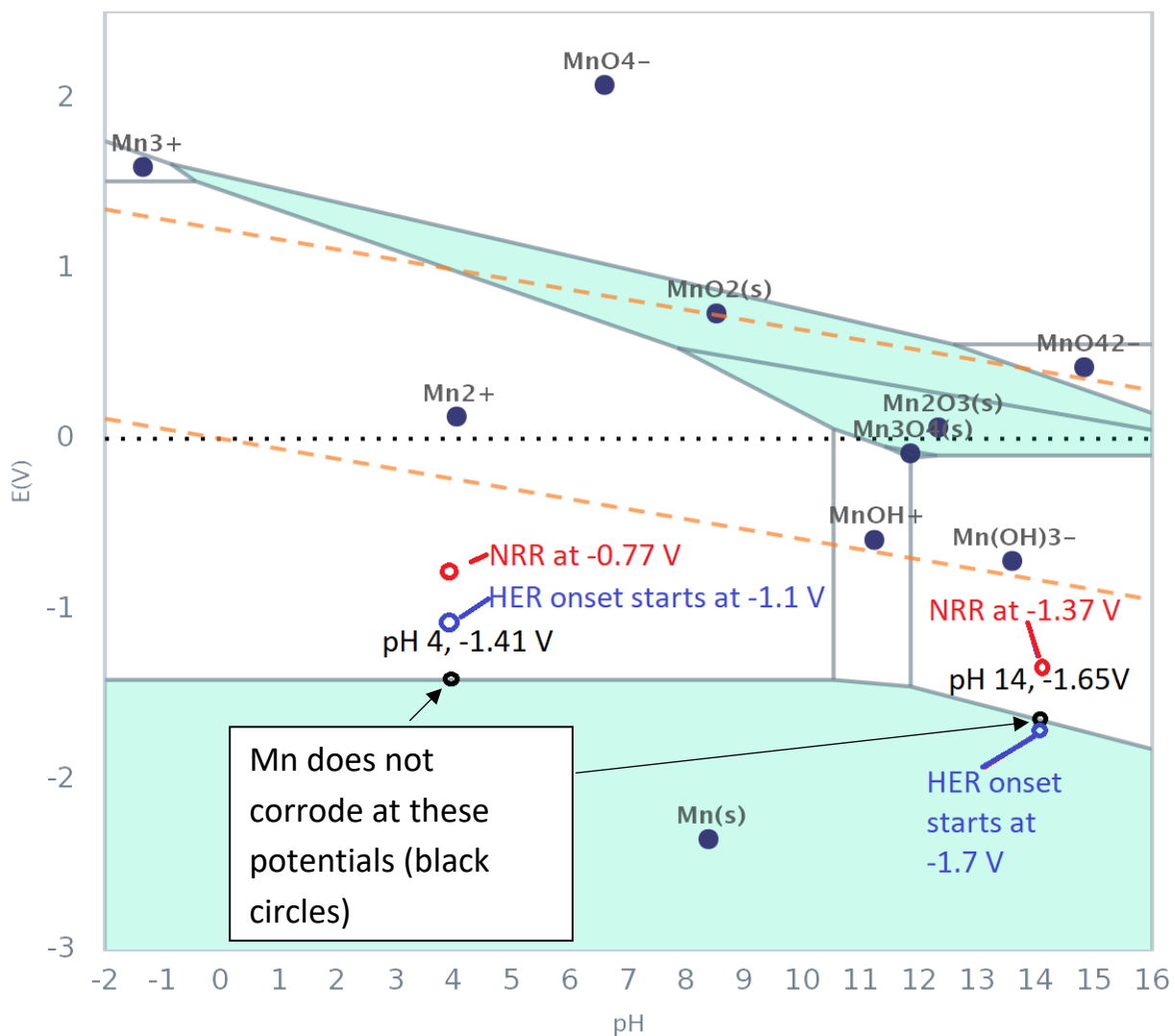


Figure S1 The Pourbaix diagram of manganese (Mn). The figure is related to Figure 5 and the discussion part titled **Thermodynamic stability of the most promising metal catalysts in water**.

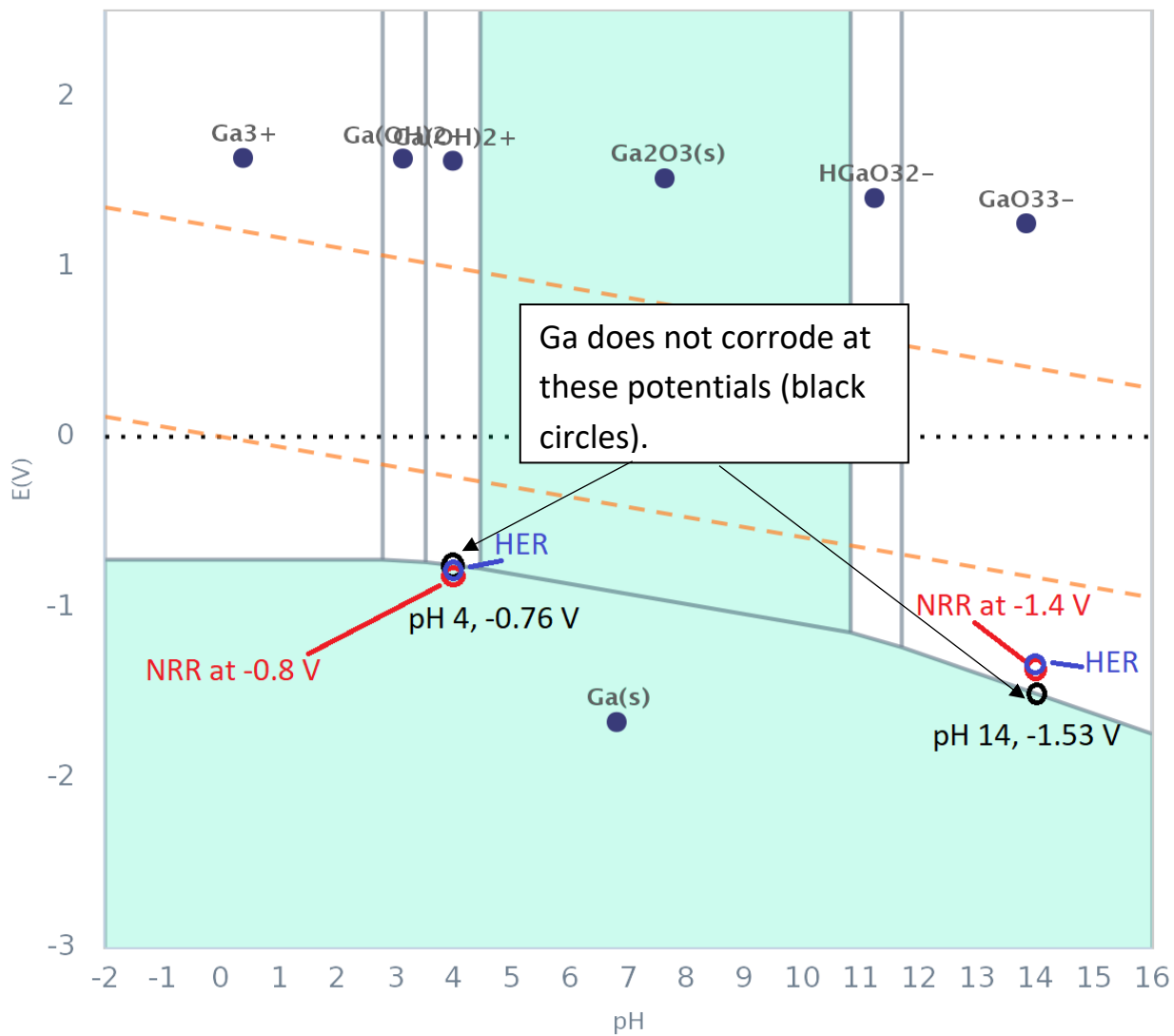


Figure S2 The Pourbaix diagram of galium (Ga). The figure is related to Figure 5 and the discussion part titled *Thermodynamic stability of the most promising metal catalysts in water.*

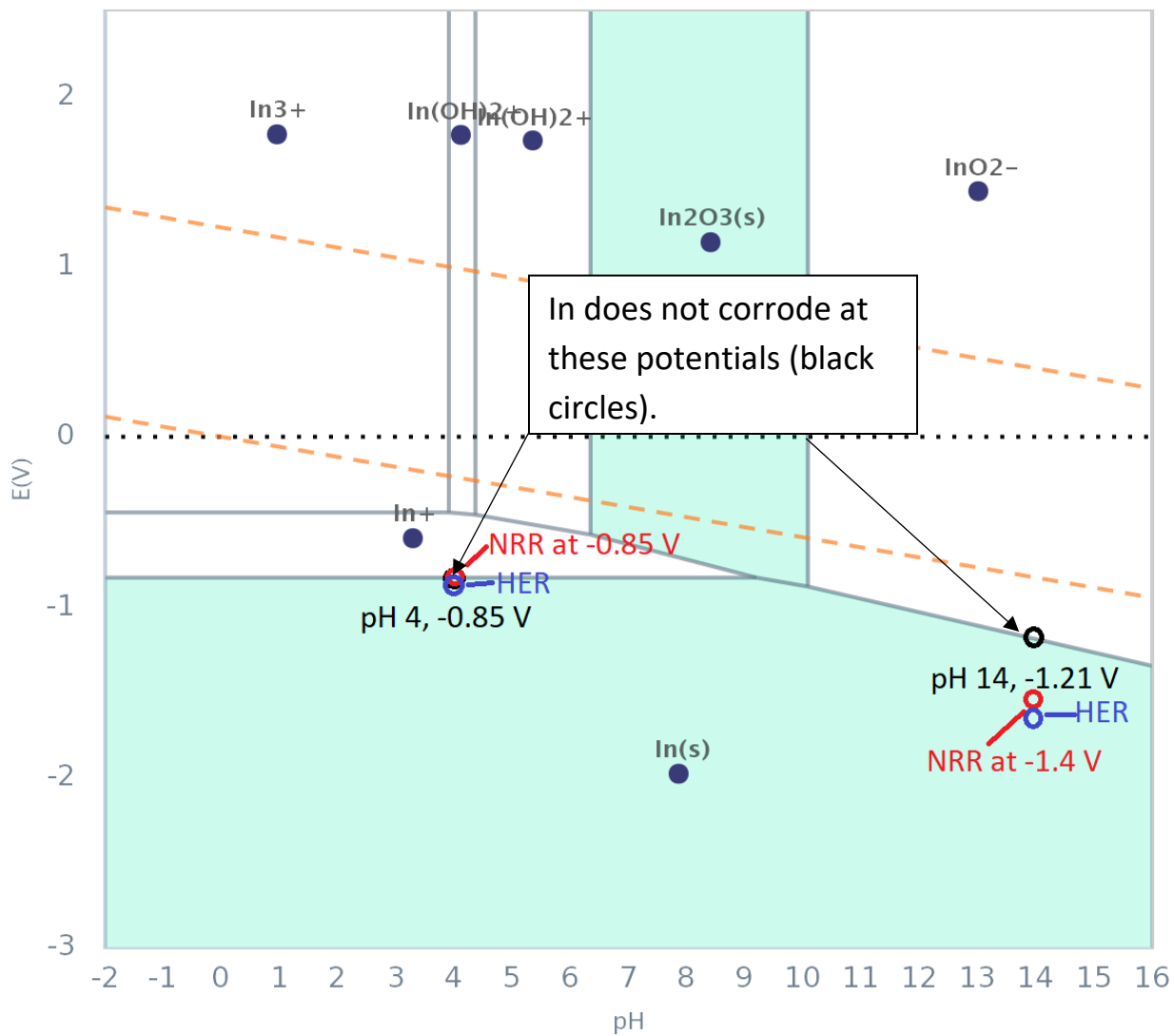


Figure S3 The Pourbaix diagram of indium (In). The figure is related to Figure 5 and the discussion part titled *Thermodynamic stability of the most promising metal catalysts in water.*

TRANSPARENT METHODS

The cell potential of M to MN reaction

The change in Gibbs free energy of the nitridation reaction can be calculated from the following cell reaction:



The standard Gibbs free energy change of the reaction (ΔG_f) in Eq. 1 is calculated as $\Delta G_f(MN, 298) = \Delta H_f(MN, 298) - T\Delta S_f(MN, 298)$, where $T = 298$ K and standard enthalpy and entropy of formation (ΔH_f and ΔS_f) of 36 MN are taken from the references (Pankratz et al., 1984, Lide, 2009). The cell reactions and corresponding stoichiometric coefficients along with all other data which we used are found in sections S3 (Table S1) and S4. The above-written cell reaction can be split in two half-cell reactions:

Cathode



Anode



The cell potential, $E_{cell}(MN)$, of an electrochemical reaction is related to ΔG_f by:

$$\Delta G_f(MN) = -nNFE_{cell}(MN) \quad (4),$$

where n is the number of moles ($n = 1$ mol), N is the number of electrons, and F is the Faraday's constant. The cell reactions found in S3 are always written so that N is 3, i.e. $\Delta G_f(MN)$ is in $\text{kJ mol}^{-1} \text{NH}_3$.

The cell potential of MN reaction with H₂ to form NH₃ and metal

In this section the cell potential of MN reaction with H₂ to form NH₃ and clean M surface is calculated. We consider the following electrochemical cell reaction:



The above-written cell reaction can be split in two half-cell reactions, where anode is the standard hydrogen electrode.

Cathode



Anode



Using the standard enthalpies and entropies of formation of MN, H₂, NH₃ and M (Pankratz et al., 1984, Lide, 2009) and stoichiometric coefficients from Eq. 5 (see SI, S3, Table S1 and S5), we calculated $\Delta G_f(\text{MN}/\text{NH}_3, 298)/\text{kJ mol}^{-1} \text{NH}_3$. Using Eq. 4 $E_{\text{cell}}(\text{MN}/\text{NH}_3)$ is calculated from $\Delta G_f(\text{MN}/\text{NH}_3, 298)$. All of the specific cell reactions considered in this section are found in SI, S5, MN to NH₃ formation reactions section. We note that the standard reduction potential on the cathode side is equal to $E_{\text{cell}}(\text{MN}/\text{NH}_3)$, when the activity of protons in solution is 1, $T = 298 \text{ K}$ and pressure of H₂ is 1 bar i.e. when anode is standard hydrogen electrode.

The potentials to start the onsets of HER and NRR at different pH

The overpotentials in HER can be calculated from exchange currents j_o (A cm⁻²) using Butler-Volmer equation (Bard and Faulkner, 2001):

$$j = j_o \left\{ \exp \left[\frac{-\alpha N F \eta}{RT} \right] - \exp \left[\frac{(1-\alpha) N F \eta}{RT} \right] \right\} \quad (8)$$

where α is the transfer coefficient, N is the number of electrons (in the case of HER it is 2), F is the Faraday's constant ($C \text{ mol}^{-1}$), R is the gas constant ($J \text{ K}^{-1} \text{ mol}^{-1}$), T is the absolute temperature (298 K) and η is the overpotential (V). The Butler-Volmer equation can be simplified and written only for the cathodic reaction, which is of interest here:

$$j_c = j_o \exp \left[\frac{-\alpha N F \eta_c}{RT} \right] \quad (9)$$

Here we use the exchange currents at pH 0 experimentally measured for many metal catalysts (Trasatti, 1972) to calculate the overpotentials at higher pH, as these are only available for a range of metals measured in a consistent way. By doing so we underestimate the HER overpotential at higher pH, as exchange currents at higher pH can be up to ten times smaller (Zheng et al., 2016). The α of HER is pH dependent (Haghighat and Dawlaty, 2016); it falls from about 0.6-0.4 at pH 0 to about 0.2 at pH 4 and is nearly constant at pH > 4. We calculated HER overpotentials (η_c) using cathodic current, j_c , of $1 \cdot 10^{-5} \text{ A cm}^{-2}$, j_o (A cm^{-2}) of HER at pH 0 from reference (Trasatti, 1972) (see SI, S7, Table S3) and took α at pH 0 in range 0.4-0.6 and for pH > 4 $\alpha = 0.2$.

η_c obtained from Eq. 9 is used to calculate the applied potential to start the onset of HER (onset potential) at a certain metal catalyst:

$$E(\text{HER, pH})/V_{\text{RHE}} = E^0(\text{SHE})/V - 0.059 * \text{pH} + \eta_c \quad (10)$$

where $E(\text{HER})$ is the HER onset potential, $E^0(\text{SHE})$ is the standard potential of hydrogen electrode, $E^0(\text{RHE})$ is the standard potential of reversible hydrogen electrode ($E^0(\text{SHE}) - 0.059 * \text{pH}$), and pH is the pH value of interest, in our case 0, 4 or 14.

NRR potential needed to start the onset of NRR (onset potential) at pH 0, 4 and 14 can be calculated using the following equation:

$$E(\text{NRR, pH})/V_{\text{RHE}} = U_L(\text{pH 0})/V_{\text{SHE}} - 0.059 * \text{pH} \quad (11)$$

where U_L is here the limiting potential for the potential determining step (PDS) of a given catalyst (Skúlason et al., 2012). U_L are taken from S6, Table S2 (most negative of the two), and by substituting these values in Eq. 11 NRR onset potential at varying pH was calculated. In case of Au, Cu, Pt, Pd and Ru, which thermochemical data on nitride formation are not available, the U_L were calculated by substituting their N-binding energies (Skúlason et al., 2012) in the following equations (Skúlason et al., 2012): i) 1st PCET $U_{L,1}(\text{Y-Fe}) = 1.61 * \Delta E(N) + 2.22$, and $U_{L,1}(\text{Fe-Ag}) = 0.59 * \Delta E(N) + 1.31$, while for 5th PCET equation $U_{L,5} = -0.33 * \Delta E(N) + 0.15$ was used. In case of Bi we used $U_L = -\Delta G_L = -2.63 \text{ V}_{\text{RHE}}$, pH 0 (Hao et al., 2019).

SUPPLEMENTAL REFERENCES

- BARD, A. & FAULKNER, L. 2001. *Electrochemical Methods - Fundamentals and Applications*, Wiley.
- HAGHIGHAT, S. & DAWLATY, J. M. 2016. pH Dependence of the Electron-Transfer Coefficient: Comparing a Model to Experiment for Hydrogen Evolution Reaction. *The Journal of Physical Chemistry C*, 120, 28489-28496.
- HAO, Y.-C., GUO, Y., CHEN, L.-W., SHU, M., WANG, X.-Y., BU, T.-A., GAO, W.-Y., ZHANG, N., SU, X., FENG, X., ZHOU, J.-W., WANG, B., HU, C.-W., YIN, A.-X., SI, R., ZHANG, Y.-W. & YAN, C.-H. 2019. Promoting nitrogen electroreduction to ammonia with bismuth nanocrystals and potassium cations in water. *Nature Catalysis*, 2, 448-456.
- JAIN, A., ONG, S. P., HAUTIER, G., CHEN, W., RICHARDS, W. D., DACEK, S., CHOLIA, S., GUNTER, D., SKINNER, D., CEDER, G. & PERSSON, K. A. 2013. The Materials Project: A materials genome approach to accelerating materials innovation. *APL Materials*, 1, 011002.
- LIDE, D. R. 2009. *Handbook of chemistry and physics*, S.I., Taylor and Francis Group.
- PANKRATZ, L. B., STUVE, J. M. & GOKCEN, N. A. 1984. Thermodynamic Data for Mineral Technology. Washington D.C.
- SKÚLASON, E., BLIGAARD, T., GUDMUNDSDÓTTIR, S., STUDDT, F., ROSSMEISL, J., ABILD-PEDERSEN, F., VEGGE, T., JÓNSSON, H. & NØRSKOV, J. K. 2012. A theoretical evaluation of possible transition metal electro-catalysts for N₂ reduction. *Physical Chemistry Chemical Physics*, 14, 1235-1245.
- TRASATTI, S. 1972. Work function, electronegativity, and electrochemical behaviour of metals: III. Electrolytic hydrogen evolution in acid solutions. *Journal of Electroanalytical Chemistry and Interfacial Electrochemistry*, 39, 163-184.
- ZHENG, J., SHENG, W., ZHUANG, Z., XU, B. & YAN, Y. 2016. Universal dependence of hydrogen oxidation and evolution reaction activity of platinum-group metals on pH and hydrogen binding energy. *Science Advances*, 2, e1501602.